CHALMERS
UNIVERSITY OF TECHNOLOGY

Implementation and Far-Field Calibration of an 8×8 37-40 GHz Phased Array with Vivaldi Aperture

Downloaded from: https://research.chalmers.se, 2026-09-15 02:33 UTC

Citation for the original published paper (version of record):
Lasser, G., Samaiyar, A., Friedrichs, G. et al (2022). Implementation and Far-Field Calibration of an 8×8 37-40 GHz Phased Array with Vivaldi Aperture. IEEE MTT-S International Microwave Symposium Digest, 2022-June: 933-936. http://dx.doi.org/10.1109/IMS37962.2022.9865257

N.B. When citing this work, cite the original published paper.

© 2022 IEEE. Personal use of this material is permitted. Permission from IEEE must be obtained for all other uses, in any current or future media, including reprinting/republishing this material for advertising or promotional purposes, or reuse of any copyrighted component of this work in other works.

(article starts on next page)

Implementation and Far-Field Calibration of an 8×8 37-40 GHz Phased Array with Vivaldi Aperture

Gregor Lasser[#,*1], Aman Samaiyar[$], Gaeron R. Friedrichs[#2], Ljubodrag B. Bosković[#], Mohamed A. Elmansouri[#], Dejan S. Filipović[#3]

[#]Department of Electrical, Computer, and Energy Engineering, University of Colorado, Boulder, USA
[$]Ansys, Inc., Boulder, USA
[*]Chalmers University of Technology, Göteborg, Sweden
[1]gregor.lasser@chalmers.se, [2]gaeron.friedrichs@colorado.edu, [3]dejan.filipovic@colorado.edu

***Abstract* — A 64 element phased array is implemented using an all metal Vivaldi aperture and 16 commercial beamforming ICs integrated on a 10-layer RF-PCB. The interconnects within the PCB are designed using circular barrels to avoid unwanted resonances, as is demonstrated by full wave simulation. The use of a non-isolated power combiner in receive mode is validated by comparing two far-field calibration techniques, resulting in measured high-fidelity beams steering up to 50°.**

***Keywords* — phased arrays, array calibration.**

I. Introduction

The push of communication systems towards millimeter wave (mmW) frequencies, particularly those for cellular 5G, has facilitated the proliferation of commercial, low-cost beam former integrated circuits (BFICs) that cover the 28 GHz or 37-40 GHz range [1], [2]. To implement a phased array antenna system, typically BFICs are integrated on a printed circuit board (PCB) which also houses the antenna elements, for which patch antennas are most commonly utilized [3]. This is undoubtedly a viable, low-cost solution for state-of-the-art communication systems, however commercial BFICs can also be used in low-cost testbeds for non-PCB based apertures.

This work investigates the use of commercial BFICs to test a high-power capable, conventionally machined, all-metal aperture for fidelity in terms of interconnection, calibration, and beam forming capabilities. The aperture is an 8×8 element Vivaldi array similar to [4], designed for operation from 10 to 40 GHz. The array is fed using 16, 4-channel, half-duplex BFICs from Anokiwave covering 37 to 40 GHz. The BFICs allow for 360° of phase control and 7.5 dB of individual gain variation per element. The aperture and BFICs are assembled into a compact, self-contained unit using a multilayer interposer PCB for RF, control, and DC supply circuits, fuzz-button interconnects, as well as an aluminium pressure and heat transfer plate that connects to an economical computer fan, see (Fig. 1a). The following sections will detail the PCB stackup and design, investigate PCB via transitions using circular barrels to avoid in-band resonances, compare two measurement-based far field calibration and beam-steering strategies and present the resulting measured receive beams up to 50° azimuth.

II. Interconnects and Printed Circuit Board

The RF interconnect between the antenna and the interposer PCB is coaxial in nature. It is based on gold plated

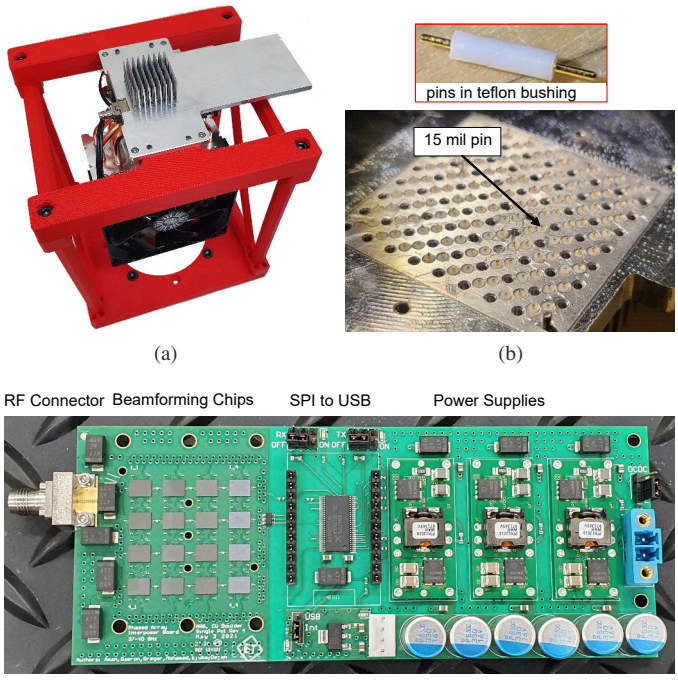

Fig. 1. Photo of the assembled array mounted in the chamber fixture (a), detail of aperture during assembly highlighting pin interconnects (b), interposer PCB view of the component side (c).

pins with 0.38 mm diameter that are seated in teflon bushings, placed inside holes of the array body, see Fig. 1b. Each coaxial transition is spring loaded with a fuzz button located in the center of the teflon bushing, pushing the pins against the Vivaldi feed points on one side and gold plated traces on the bottom side of the PCB, see Fig. 1c.

The packaging of the BFICs using solder balls with 0.4 mm pitch requires precise execution in the layout and manufacturing processes. The choice of PCB stackup (Fig. 2) is therefore influenced by RF design considerations, required DC and control signal routing layers, and overall manufacturability. The substrate used is i-Tera MT40 from isola. It is a low loss material with good RF performance but was chosen primarily for its excellent mechanical properties required for the complicated stackup. Permittivity and loss tangent of the individual dielectric layers are shown in Fig. 2. The top

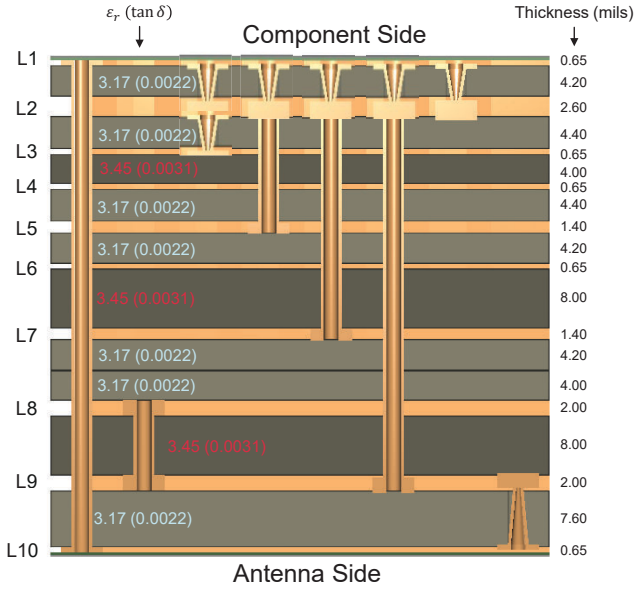

Fig. 2. PCB Stackup, and via options, substrates are isola I-Tera MT40.

L1 metal layer holds all electronic components and employs microvias to connect to layer L2 below. Keeping the copper plating cycles on the top layer low allows for a ground plane on most of the top layer while maintaining sufficient clearance to the solder ball pads for the BFICs. Most of the RF routing is implemented in stripline in layers L7 and L9, where layers L6, L8 and L10 are acting as ground planes. Layers L2-L5 are used for control and power distribution.

A. RF Routing and Via Transitions

The combined RF signal enters the board at a 2.9 mm connector on the top layer as a grounded CPW trace. It then transitions to L7 where it feeds an non-isolated combiner implemented in stripline as shown in Fig. 3a. The combiner feeds the 16 common ports of the BFICs that in turn each feed four antenna ports. Since the BFICs are larger than the 4 mm element to element spacing of the array aperture, the RF lines feeding the antennas need to be routed under the BFICs, which is accomplished on layer L9. The transitions from L1 to layers L7 and L9 needs to be designed to avoid mismatch and radiation, so they were investigated in a separate simulation study. Using a simple single via for the interconnect creates multiple resonances and significant associated loss, as shown in Fig. 4. The opposing direction of the match in $|S_{11}|$ and $|S_{22}|$ at the resonances shows that the signal is radiated into the substrate and not just reflected, which could be cured by transmission line matching sections in layers L1 and L9. We therefore implement shielding barrels (see Fig. 3b) to create a quasi coaxial transition, which improves return loss and eliminates all resonances below 40 GHz.

III. Calibration and Beamforming

Phased arrays typically require calibration to eliminate amplitude and phase errors at the element level to obtain clean

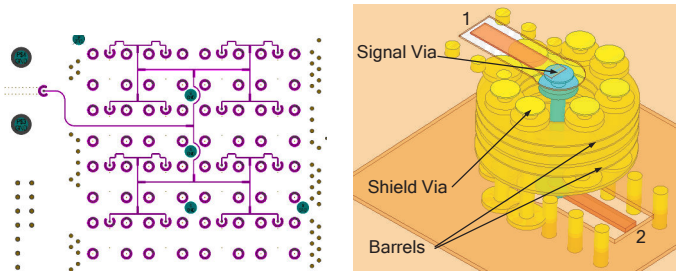

Fig. 3. RF power combiner implemented as stripline circuit on Layer 7, using vias with barrel ground rings (a), single via CPW (L1) to stripline (L9) transition using ground barrels (b).

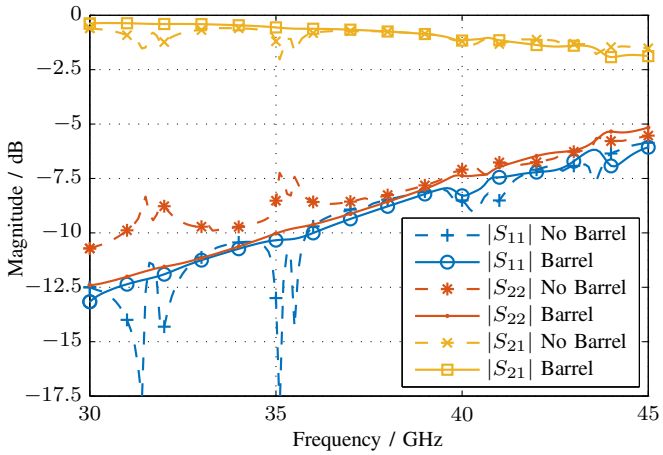

Fig. 4. Simulation of the RF transition from layer 1 (grounded CPW) to layer 9 (stripline) using the port definitions as shown in Fig. 3b.

beams. For electronically scanned arrays, the main sources of error are the signal distribution network, BFIC characteristics, and beamformer to antenna element feed [3]. At lower operating frequencies it is possible to avoid calibration entirely by careful design and stable factory-calibrated chips [5], but this fails at high frequencies. Therefore, calibration methods utilizing the antenna element to element coupling are used [3], [6]. Since a non-PCB based aperture is used in this work and the interconnects involve unstable mechanical spring contacts, an internal calibration method is unusable. Instead, a far-field calibration technique [7] is implemented as described next.

A. Calibration Method Comparison

The phased array is placed in an anechoic chamber, and measured in receive mode at boresight for a frequency range from 35 to 43 GHz using a vector network analyzer. For this measurement, only a single antenna element is measured at a time by commanding the BFICs to deactivate all channels except one, which is set to 0° of phase shift and no attenuation. This yields the individual frequency responses of all 64 elements. A calibration frequency (39.8 GHz) is selected to find the required amplitude and phase settings of the BFICs to equalize the antenna signals. Fig. 6a shows the maximum amplitude deviation of this initial measurement

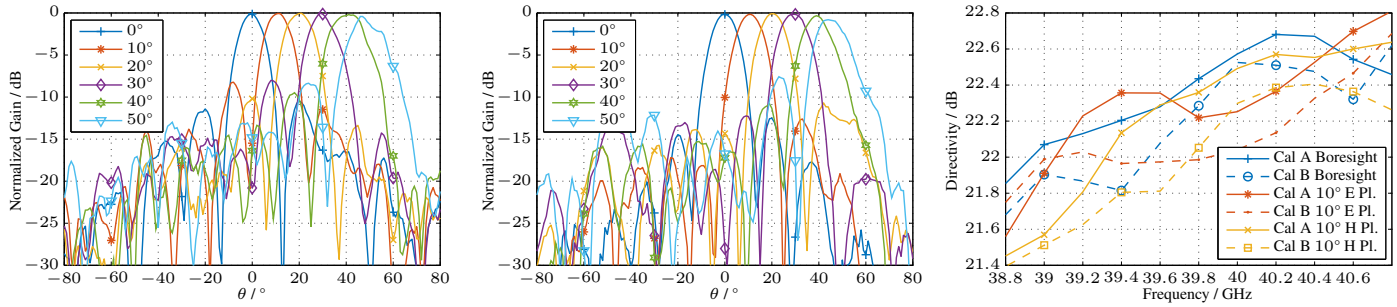

(a) (b) (c)

Fig. 5. Measured E-plane (a) and H-plane (b) cuts at 39.8 GHz using Cal A; directivity for boresight and 10° steered beams comparing Cal A and Cal B (c).

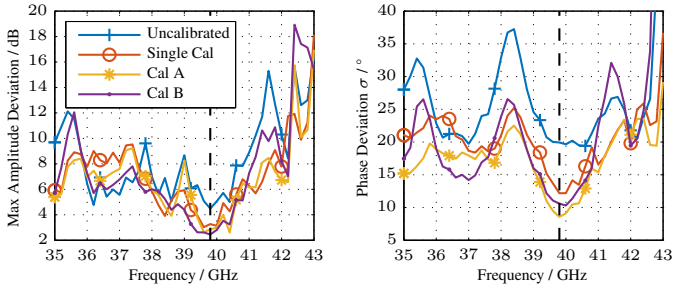

(a) (b)

Fig. 6. Maximum amplitude deviation (a), and standard deviation of phase distribution (b) of the phased array calibration measurements, the dashed line indicates the calibration frequency of 39.8 GHz.

and the subsequent test measurement of the applied single calibration. Fig. 6b shows the standard deviation of the phase measurements when a normal distribution is fitted to the data. We note that the initial calibration improves the maximum amplitude deviation at the calibration frequency from 4.5 dB to 3.3 dB, and the standard deviation of the phase from 19.9° to 12.2°.

We then repeat the calibration by again measuring all 64 elements individually at boresight, but now setting each amplitude and phase to the equalization values found before. For the resulting second calibration we compare two strategies called 'Cal A' and 'Cal B'. Both methods equalize the individual elements based to the mean amplitude and phase as found in the previous measurement of the 'Single Cal'. For Cal A we additionally add a constant phase shift to all elements such that for a boresight beam no wrapping around 360° occurs. Fig. 6a shows that both methods improve the maximum amplitude deviation further, with Cal B we see the best result at the calibration frequency of a maximum amplitude deviation of 2.5 dB, Cal A is slightly worse because more BFIC phase states are changed. However, Cal A shows a lower phase deviation (Fig. 6b) and is chosen for the swept beam measurements.

IV. Pattern Measurements

The calibrated array is swept in the E and H plane without any amplitude taper using ideal steering coefficients and measured in receive mode in an anechoic chamber. Amplitude and phase values are corrected based on the Cal A data explained before, which for steering angles below 15° results in a phase progression on the BFICs not wrapping around 360°. Beams steering up to 50° in azimuth are shown in Fig. 5. The beams are clean and the E-plane sidelobes when scanned up to 50° remain below 8.0 dB although a non-isolated combiner is used in receive, which can lead to spurious lobes due to reflections in the combiner that can end up at the common output port. This effect of the non-isolated combiner can also not be fixed using array calibration. At H-plane the sidelobes remain below 10.8 dB scanning up to 40°.

To further evaluate the effect of the calibration on the beam shape we compare the measured directivity of beams at boresight and 10° steered in the E and H-plane for both calibration strategies, see Fig. 5c. We observe that for all beams the directivity obtained with Cal A exceeds the one from Cal B from 39.1 GHz to 40.8 GHz.

V. Conclusion

We present an 8×8 phased array based on an all-metal Vivaldi antenna aperture connected to commercial beam forming chips using a multilayer RF interposer PCB and spring loaded pins. The 16-fold power combiner implemented in stripline is connected to the top PCB layer using barreled via interconnects to avoid resonances and radiation losses. The presented far-field calibration and beamforming strategy improves element accuracy and directivity by avoiding phase wrapping over 360°. Without amplitude tapering, clean beams with sidelobe levels below 8 dB are demonstrated up to 40° scanning in E and H-planes.

Acknowledgment

The authors would like to acknowledge the financial support for this work by L3Harris.

References

[1] A. G. Roy, O. Inac, A. Singh, T. Mukatel, O. Brandelstein, T. W. Brown, S. Abughazaleh, J. S. Hayden, B. Park, G. Bachmanek *et al.*, "A 37-40 GHz phased array front-end with dual polarization for 5G MIMO beamforming applications," in *2019 IEEE Radio Frequency Integrated Circuits Symposium (RFIC)*. IEEE, 2019, pp. 251–254.

[2] C.-N. Chen, Y.-H. Lin, Y.-L. Liu, W.-J. Liao, Y.-H. Nien, H.-C. Lu, T.-H. Tsai, T.-W. Huang, and H. Wang, "36–40 GHz Tx/Rx beamformers for 5G mm-wave phased-array," in *2018 Asia-Pacific Microwave Conference (APMC)*. IEEE, 2018, pp. 756–758.

[3] Y. Wang, R. Wu, J. Pang, D. You, A. A. Fadila, R. Saengchan, X. Fu, D. Matsumoto, T. Nakamura, R. Kubozoe *et al.*, "A 39-GHz 64-element phased-array transceiver with built-in phase and amplitude calibrations for large-array 5G NR in 65-nm CMOS," *IEEE J. Solid-State Circuits*, vol. 55, no. 5, pp. 1249–1269, 2020.

[4] M. A. Elmansouri, G. R. Friedrichs, L. B. Boskovic, and D. S. Filipovic, "An X-through Ka-band thinned all-metal Vivaldi phased array," *IEEE Trans. Antennas Propag.*, 2021.

[5] K. Kibaroglu, M. Sayginer, T. Phelps, and G. M. Rebeiz, "A 64-element 28-GHz phased-array transceiver with 52-dBm EIRP and 8–12-Gb/s 5G link at 300 meters without any calibration," *IEEE Trans. Microw. Theory Techn.*, vol. 66, no. 12, pp. 5796–5811, 2018.

[6] A. Nafe, K. Kibaroglu, M. Sayginer, and G. M. Rebeiz, "An in-situ self-test and self-calibration technique utilizing antenna mutual coupling for 5G multi-beam TRX phased arrays," in *2019 IEEE MTT-S International Microwave Symposium (IMS)*. IEEE, 2019, pp. 1229–1232.

[7] R. Sorace, "Phased array calibration," *IEEE Trans. Antennas Propag.*, vol. 49, no. 4, pp. 517–525, 2001.